Carbon 152 (2019) 89–97

Contents lists available at ScienceDirect

Carbon

journal homepage: www.elsevier.com/locate/carbon

Bimodal porous carbon cathode and prelithiated coalesced carbon onion anode for ultrahigh power energy efficient lithium ion capacitors

Amir Reza Aref [a], Shih-Wen Chen [b], Ramakrishnan Rajagopalan [c, d, *], Clive Randall [b, d]

[a] Department of Engineering Science and Mechanics, The Pennsylvania State University, University Park, PA, 16802, USA
[b] Department of Materials Science and Engineering, The Pennsylvania State University, University Park, PA, 16802, USA
[c] Department of Engineering, Penn State DuBois, DuBois, PA, 15801, USA
[d] Materials Research Institute, The Pennsylvania State University, University Park, PA, 16802, USA

ARTICLE INFO

Article history:
Received 16 April 2019
Received in revised form
21 May 2019
Accepted 27 May 2019
Available online 30 May 2019

Keywords:
Lithium ion capacitor
High rate anode
Hierarchical porous carbon
Carbon onions
Bimodal porous carbon

ABSTRACT

Lithium ion capacitors made using prelithiated coalesced carbon onion based anode showed excellent high energy and power performance with time constant in the order of ~1.45s. The interconnected carbon onion microstructure facilitated both rapid electron and ion transport thereby minimizing the overall resistance. Additionally, high specific capacitance was achieved through control of pore size distribution in high surface area carbons derived from polyfurfuryl alcohol based polymer blends. The fabricated capacitors can be charged and discharged in less than 30s between 2.2V – 4V with energy efficiencies >90%. The maximum achievable energy density was 120 Wh/kg with the capacitor retaining 77 Wh/kg even at a high power density of 11 kW/kg. The capacitors also demonstrated excellent cycling stability with 80% capacitance retention over 21000 cycles along with good thermal stability up to 60 °C.

1. Introduction

Lithium-ion capacitor (LIC), a hybrid supercapacitor comprising of high surface area carbon cathode and a lithium ion battery anode, is one of the most promising energy storage devices as they provide high power density, long cycle life, and good energy storage performance [1]. In the hybrid LIC device, charge storage occurs due to non-Faradaic electrochemical double layer adsorption of ions on the cathode along with faradaic lithium intercalation in the anode electrode [2,3]. This integrated design allows us to achieve higher energy density than EDLC and increased working voltage [3]. Despite many advantages of this design, there are critical challenges that need to be overcome that include a mismatch of charge storage and rate capability of battery type anode and double layer cathode. The energy density of the device is thus limited by non-Faradaic double layer storage mechanism in the positive electrode while the rate capability of the device is restricted by the sluggish Li^+ intercalation kinetics in the negative electrode. The problem is further compounded by severe mass transfer limitations at higher load current densities in both the electrodes.

Various allotropes of carbon that include graphite, porous carbon, graphene and carbon nanotube form the basic building block of both anode and cathode electrode architecture [4,5]. The performance of LIC is closely related to both the textural and microstructural properties of these carbons. To boost charge storage capacity of cathode material, the main strategies adopted are to maximize available surface area through pore size optimization by matching the pore size relative to electrolyte ion size [6,7]. Additionally, the use of reversible pseudocapacitive interaction (mainly through reversible Li^+ interaction with functional groups such as pyridinic and carbonyl) with electrode material as well as doping of the electrode material to improve conductivity has also been attempted [8,9].

High rate capability (>2C) of lithium interaction with graphite anode is mainly determined by the tortuosity and hence the microstructure of the electrode. Two major microstructural features of the electrode that include particle size and porosity influences this performance. Buqa et al. developed a transport limitation model to explain the restrictions of high current performance of synthetic

* Corresponding author. Department of Engineering, Penn State DuBois, DuBois, PA, 15801, USA.
E-mail address: rur12@psu.edu (R. Rajagopalan).

https://doi.org/10.1016/j.carbon.2019.05.074
0008-6223/

graphite electrodes. They showed that by tailoring the graphite particle size, it was possible to maintain 96% capacity retention even at 20C rate [10]. A physico-chemical model has been developed by Habedank et al. who demonstrated three stages of rate influence on synthetic graphite anode by engineering laser structured transport pores [11]. At low rates (<1C), the capacity was influenced by ohmic losses and charge transfer kinetics. Between 1C and 4C, the performance became more sensitive to microstructural features such as porosity. The presence of porosity ensured that there is more homogeneous liquid and solid phase concentration of lithium ions resulting in better capacity retention at these rates. At even higher rates, the microstructural features had lesser impact and the performance was dominated by large depletion of Li ions in the pores causing huge overpotentials. In LIC design, the mass of cathode is always greater than that of anode and due to this the graphite anode always experiences higher current density and the performance of the graphite at higher rates (second and third stage) inevitably determines the power performance of the capacitor.

Among the various carbon forms, fullerene based carbon nanostructures such as carbon onions provides the best morphology for use as high rate anodes as their average primary particle size range in the order of 4–25 nm and they also possess well interconnected porosity. The electrical properties of these carbon onions are however dependent upon their synthesis conditions which may be through detonation method, vacuum annealing, arc discharge, CVD or laser excitation process [12–21]. Carbon onion based supercapacitors have been primarily reported for aqueous based electrolytes and microsupercapacitors with rate capability as high as 50 V/s and small time constant of ~26 ms [22]. The use of these materials in non-aqueous lithium based electrolytes for use in lithium ion capacitors have not been well explored so far and warrants a detailed investigation. In particular, the concentric graphitic shells in carbon onions can provide excellent electrical conductivity along with larger surface area for electrochemical interaction with lithium facilitating both rapid ion transport and charge transfer during charging and discharging. The major challenge that needs to be addressed is in terms of SEI formation/stabilization and irreversible lithium loss during initial cycling. This problem can however be mitigated using a prelithiation process that can result in a well passivated anode prior to the assembly of lithium ion capacitors.

Herein, we demonstrate a high rate all carbon based lithium ion capacitor (LIC) that is capable of being charged and discharged with excellent cyclability and good temperature stability. The remarkable performance of the lithium ion capacitor is due to the use of coalesced carbon onion based anode and a high surface area bimodal porous carbon cathode. The hybrid LIC capacitor had outstanding rate and energy efficiency performance with discharge time ~30 s and cycle life of 80% capacitance retention over 21000 cycles.

2. Experimental section

All the chemicals including furfuryl alcohol, p-toluenesulfonic acid monohydrate, Polyethylene Glycol (Mw 8000 g mol^{-1}), Polyethylene Glycol diacid ((Mw 600 g mol^{-1}), pluronic F127, formaldehyde, and electrolyte solution contained 1 M $LiPF_6$ in EC/DMC (1:1 by volume) were purchased from Sigma-Aldrich. Additionally,

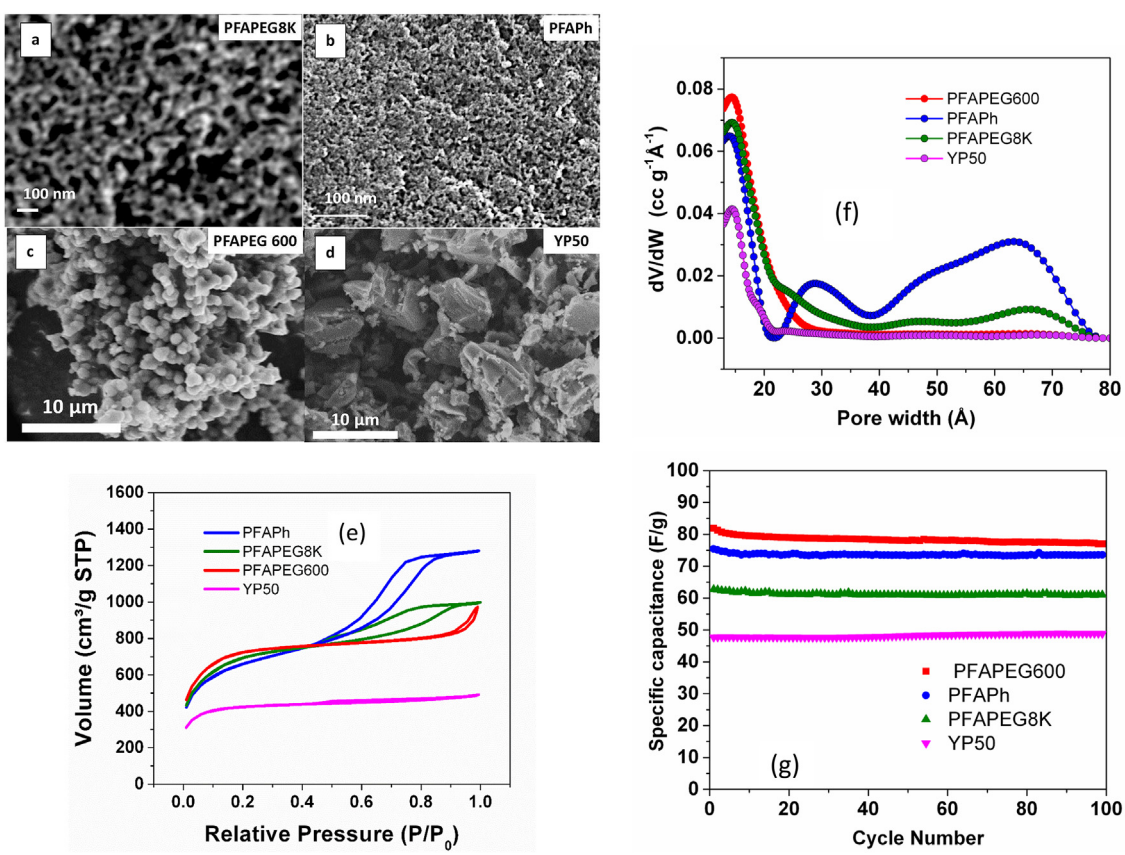

Fig. 1. SEM showing morphology of various cathode carbons: (a) PFA_PEG600, (b) YP50, (c) PFA_Ph, (d)PFA_PEG8K, (e) Adsorption/Desorption nitrogen isotherm of various carbons, (f) NLDFT model showing micropore and mesopores size distribution of the carbons, and (g) specific capacitance of Lithium ion capacitors made using aforementioned activated carbon cathodes and prelithiated CMS Graphite anode measured at a current density of 0.1 A/g when charged and discharged between 2.2V–4.5V

Table 1
Textural properties of the carbons.

Activated Carbon	Surface area (m^2/g)	Micropore volume (cc/g)	Mesopore volume (cc/g)	Total volume (cc/g)
PFA_Ph	2320	0.37	1.29	1.98
PFA_PEG600	2578	0.61	0.25	1.50
PFA_PEG8K	2450	0.38	0.65	1.54
YP50	1599	0.47	0.12	0.76

two different anode materials namely coalesced carbon onion (CCO) and MCMB graphite were purchased from ACS material and MTI corporation, respectively.

2.1. Synthesis of activated carbon cathode material

Polyfurfuryl alcohol (PFA) was synthesized by acid polymerization of furfuryl alcohol using 0.1 M p-toluenesulfonic acid monohydrate (Sigma-Aldrich) as acid catalyst. Two carbons with different porous texture namely PFA_PEG8K and PFA_PEG600 were prepared by blending the synthesized polyfurfuryl alcohol with polyethylene glycol (MW: 8000 g mol^{-1}) at a wt. Ratio of (3:1) and polyethylene glycol diacid (MW:600 g mol^{-1}) at a wt. Ratio of 1:2, respectively. Additionally, PFA_Ph was synthesized by simultaneous polymerization of furfuryl alcohol and phloroglucinol using pluronic F127 as a soft templating agent [23–26]. Briefly, 20 mmol of Phloroglucinol, 0.2 mmol of pluronic F127 and 2 mmol of HCl was dissolved in ethanol/water (1:1 wt Ratio). The solution was allowed to stir for 1 h followed by addition of 10 mmol furfuryl alcohol. The reaction continued for 30 min until the color changed to light pink. To this solution, 30 mmol formaldehyde was added and the mixture was stirred until phase separation occurred. The polymer rich phase was separated and the polymerization was continued overnight. The resultant polymers were dried in an oven at 90 °C overnight and carbonized under argon atmosphere at 800 °C for 8 h. The carbons were further physically activated using CO_2 gas at 900 °C for a defined period of time in order to achieve high surface area carbon with 75% burn off.

2.2. Electrode preparation and fabrication of cells

For cathode materials, the synthesized high surface area carbon (PFA, PFA_PEG8K, PFA_PEG 600, and PFA_Ph) were mixed with 5% acetylene black, 10% Teflon emulsion using mortar and pestle. The resultant mixture was roll pressed and punched in a circular shape with 1.1 cm diameter and a mass loading of ~ 5 mg. For anode electrode, commercial carbon onion (purchased from ACS material Inc.) was mixed with CMC and SBR binder, acetylene black, and water as a solvent in the weight ratio of 85:10:5 to get a homogenous slurry. Then the slurry was tape casted on the copper foil and dried in an oven at 100 °C overnight and then in vacuum at 100 °C for 10 h. Finally, the electrodes were punched in circular shape with 1.1 cm diameter with mass loading of ~ 2 mg. Before assembling, the anode electrode was prelithiated using short circuiting approach during which the anode foil was pressed against lithium foil in the presence of 1 M LiPF6 in EC/DMC (1:1 by volume)

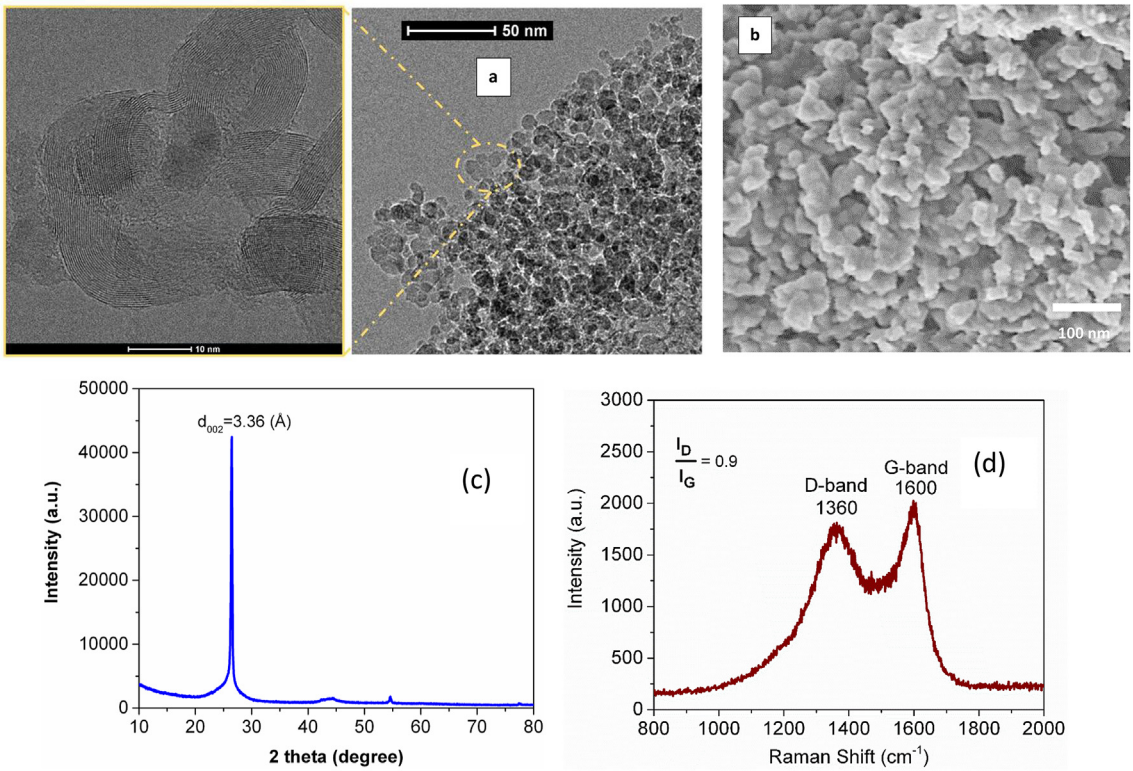

Fig. 2. (a) TEM image of coalesced carbon onion; High resolution image of carbon onion from the selected region (shown as Inset), (b) Field Emission SEM image showing the morphology of fused carbon onion, (c) XRD of carbon onion indicating the presence of graphitized domains, and (d) Raman spectra of coalesced carbon onion.

electrolyte for 1 day to form a prelithiated anode with well stabilized SEI layer. All the capacitors were then assembled into a 2032 coin cell using 1 M LiPF6 in EC/DMC (1:1 by volume) electrolyte in an inert glove box atmosphere. In addition, YP50 coconut shell based carbon, was purchased from Kuraray Chemical Co. Was used for comparison. The main reason for synthesizing different types of activated carbons with distinct pore size distribution was to investigate the impact of pore size distribution in the rate and charge storage performance of lithium ion capacitor.

2.3. Characterization methods

The specific surface areas and pore-size distributions (PSD) of the samples were computed using gas adsorption studied with Micromeritics ASAP 2020 Plus instrument. The surface area was computed and analyzed using the Brunauer-Emmett-Teller (BET) method and the pore size distribution was obtained using nonlinear density functional theory (NLDFT) fitted model on the N_2 adsorption isotherm, respectively [27]. The microstructure of carbon onion was analyzed using a Renishaw inVia Raman spectrometer with the 514 nm laser line and PANalytical Empryean X-ray diffractometer. The morphology of the coalesced carbon onion was further studied using scanning electron microscopy (FESEM, JEOLJSM 7200 F) and Transmission electron microscopy (TEM, Talos F200X).

2.4. Electrochemical measurements

Gamry reference 600 potentiostat/galvanostat was used for all electrochemical measurements including Galvanostatic charge-discharge (GCD) and electrochemical impedance spectroscopy (EIS). Energy density (Wh/kg), power density (W/kg), and Specific capacitance (F/g) were calculated according to $E = \frac{I\int_{t_1}^{t_2} Vdt}{m*3.6}$, $P = \frac{3600\ E}{\Delta t}$, and $C = \frac{3.6*E}{0.5\ (V_2^2 - V_1^2)}$, respectively. Where I is current in A, and Δt is the discharge time in second, m is the total mass of active material from both anode and cathode electrodes in g, V2 is the upper potential limit and V1 in lower potential limit from the discharge profile. EIS was conducted by applying small amplitude of 10 mV under open circuit conditions in the frequency range of 1 mHz–100 KHz.

3. Results and discussion

Fig. 1a–d shows the comparison of SEM morphology of the different high surface carbons used as cathode. PFA_PEG8K and PFA_Ph shows dense microstructure with interconnected mesoporous texture. PFA_Ph showed mesoporosity in the range of 5–10 nm while PFA_PEG8K demonstrated slightly larger pores (Fig. 1a and b). PFA_PEG600 predominantly had spherical morphology with primary particle size in the range of 100 nm (Fig. 1c). On the other hand, commercial YP50 carbon has a flaky morphology with particle size in the range of 10 μm. Fig. 1e shows the N_2 adsorption/desorption isotherm of various carbons. Both PFA_PEG8K and PFA_Ph show hysteresis in the isotherm and a plateau at very high relative pressures that is indicative of presence of large amount of mesopores and is typical of a type IV adsorption isotherm. PFA_PEG600 show relatively no hysteresis with a steep increase in adsorption both at very low and very high relative pressures, representing a type II adsorption isotherm. Type II adsorption curve shows the presence of both micropores and macropores in this carbon. YP50 also shows no hysteresis and is representative of Type I isotherm with sharp increase in adsorption at very low relative pressures and an adsorption plateau at higher relative pressures. This carbon is essentially a pure microporous carbon. NLDFT analysis done in the pore size range of 1–10 nm demonstrate the presence of ultramicropores for all the carbons (Fig. 1f). Both PFA_Ph and PFA_PEG8K show the presence of mesopores in this range while YP50 and PFA_PEG600 do not show significant mesoporosity. The mesopore distribution for PFA_Ph is very prominent indicating a distinct bimodal porous feature in both micropore (<2 nm) and mesopore region (3–10 nm). On the other hand, PFA_PEG8K had a fairly broad distribution in this range. Table 1 summarizes the textural properties of all the carbons. Notably, PFA_PEG600 had the largest amount of micropore volume (0.6 cc/g) followed by YP50 (0.47 cc/g) and PFA_PEG8K and PFA_Ph (~0.37 cc/g). The mesopore volume was significantly larger for PFA_Ph (1.29 cc/g) followed by PFA_PEG8K, PFA_PEG600 and YP50. The surface area for YP50 was 1600 m^2/g while that of PFA_PEG600, PFA_PEG8K and PFA_Ph was 2578 m^2/g, 2450 m^2/g and 2320 m^2/g, respectively.

The distinct morphology and textural properties of the polyfurfuryl alcohol blend precursors is due to the reaction induced phase separation phenomena that occurs during thermal treatment of the precursors. Specifically, the pore size distribution of

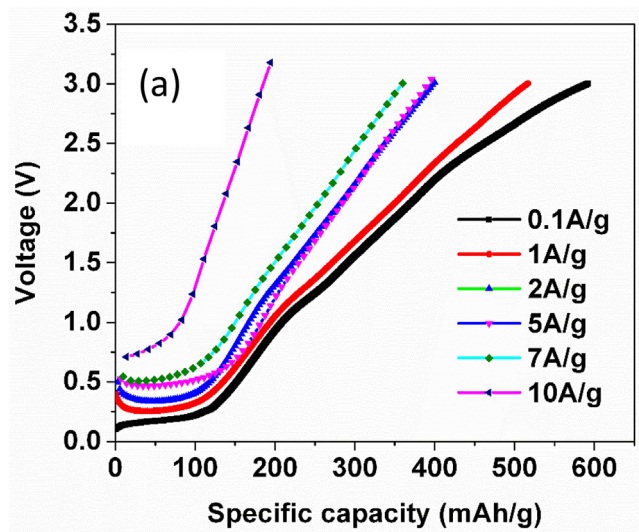

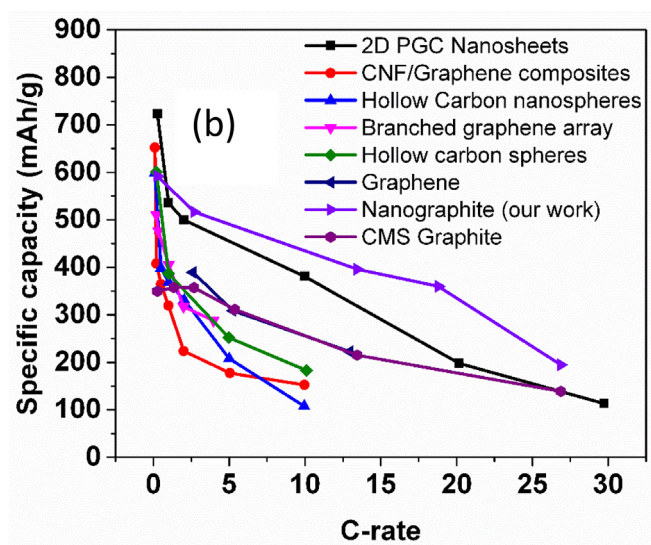

Fig. 3. (a) Half-cell study of prelithiated carbon onion anode when delithiated at different current densities, (b) Capacity retention as a function of C-rate of Carbon onion anode (our work) when compared to other carbon-based anodes.

PFA_PEG8K is affected by the phase separation of PFA rich region that predominantly forms the micropore network while decomposition of PEG8K rich region forms the mesopore. In the case of PFA_Ph, both PFA and Ph contribute to micropore formation while a triblock copolymer surfactant (Pluronic-F127) produces a templating effect resulting in well-ordered mesoporous texture and hence bimodal pore size distribution. In the case of PFA_PEG600, PEG600 acts more like a solvent that induces micelle formation. The solvent phobic pendant groups in polyfurfuryl alcohol forms the core of the micelle which eventually upon pyrolysis transforms into a microporous carbon sphere with the excess PEG600 flashing off to form macrovoids.

The impact of porosity on the performance of the capacitor can be seen in Figure 1g. All the capacitors were assembled using a prelithiated commercial MCMB graphite (~20 μm particle size) and the mass ratios of cathode: anode was ~2:1. PFA_PEG600 with its large amount of micropore volume showed the highest capacitance of 78 F/g at 100 mA/g when cycled between 2.2V–4.5V. The texture of the carbon had significant effect on electrolyte accessibility as the primary particle size of the carbon was ~100 nm and was surrounded by large macropores. In comparison, YP50 cathode, also made using a predominantly microporous carbon with particle size of ~10 μm had a specific capacitance of 48 F/g. The performance of PFA_Ph and PFA_PEG8K with micro- and mesopores ranged in between these carbons. The maximum achievable energy density at 300 W/kg was ~160 Wh/kg.

Several research studies have shown that specific capacitance always enhances when the electrolyte ion size matches with pore size of the electrodes [28]. Furthermore, molecular dynamic simulation show that the solvated PF_6^- in EC/DMC has diameter ~0.9 nm [29]. Our observation are in agreement with the literature as PFA_PEG 600 showed both the highest micropore volume in the ultramicropore region (0.8–2 nm) as well as the largest specific capacitance. However, the specific capacitance of the carbon decreased significantly with increase in current density. When we compare the micropore volume of YP50 and other carbons, it was evident that the presence of mesoporosity is critical in determining the accessible surface area at a given current density. YP50, being predominantly a microporous carbon showed the smallest capacitance while the trend in specific capacitance of PFA_Ph and PFA_PEG8K with similar micropore volume was determined by the amount of mesoporosity. Hence, for our high rate studies with carbon onion based anode, we chose PFA_Ph among the three synthesized carbons as it provided the best rate and optimum capacitance performance.

Transmission electron micrograph image of the anode material revealed a carbon onion structure with a primary particle size in the order of 10–15 nm. The particles appear coalesced forming a beaded structure as shown in Fig. 2a. We also saw further evidence of coalescence through SEM micrograph as shown in Fig. 2b. Moreover, the spherical morphology of the carbon onion anodes also created small nanopores in the carbon onion clusters. This intrinsic porous texture provides both good accessibility of the lithium ion electrolyte as well as significantly shortens the ion diffusion pathway in the anode. The coalesced microstructure may also be critical to the electronic conductivity of the carbon onion anode. XRD showed a distinct (002) peak with d-spacing of 3.36 Å indicating the presence of well graphitized domains (Fig. 2c) in the carbon onion microstructure. This is also in good agreement with our TEM observation (Fig. 2a). The crystallite size of the peak as calculated using the Scherrer equation was ~42 nm. Considering the primary particle size of the onions was ~10 nm, this shows further

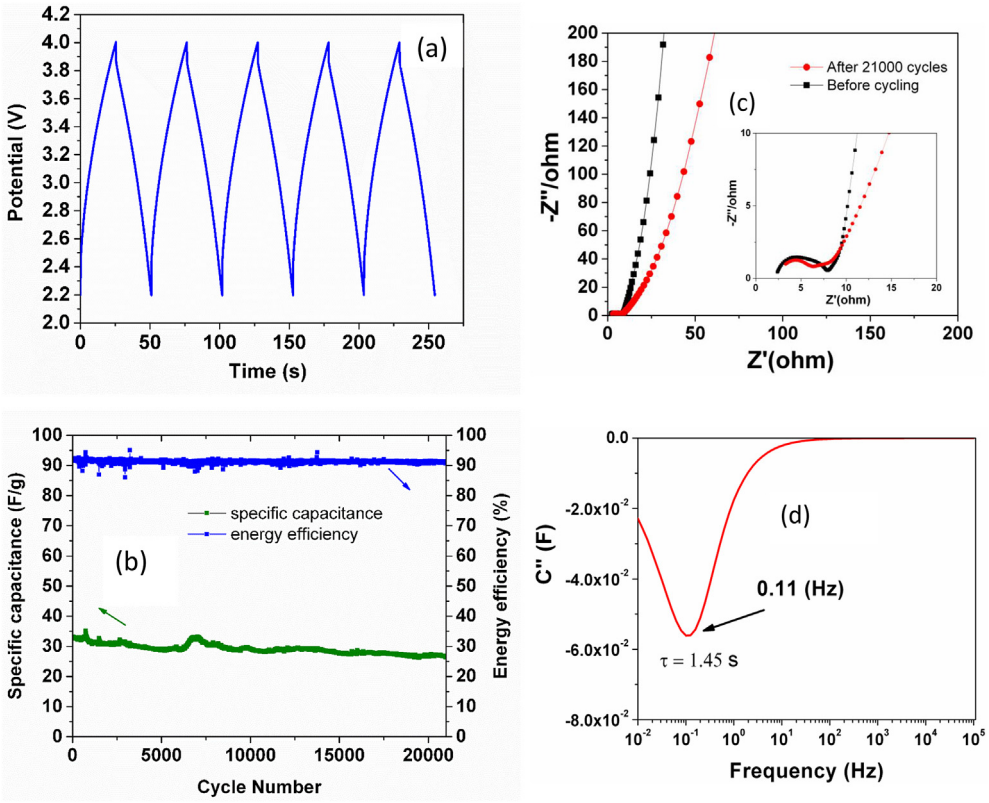

Fig. 4. (a) Long term cycling study of PFA_Ph/CCO Lithium ion capacitor showing both change in specific capacitance as well as energy efficiency when cycled between 2.2V and 4 V at 2A/g, (b) Constant current charge-discharge profile when cycled between 2.2V and 4V at 2 A/g, (c) Nyquist plot of capacitor measured before and after cycling, and (d) imaginary capacitance versus frequency plot of capacitor showing a time constant of 1.45s.

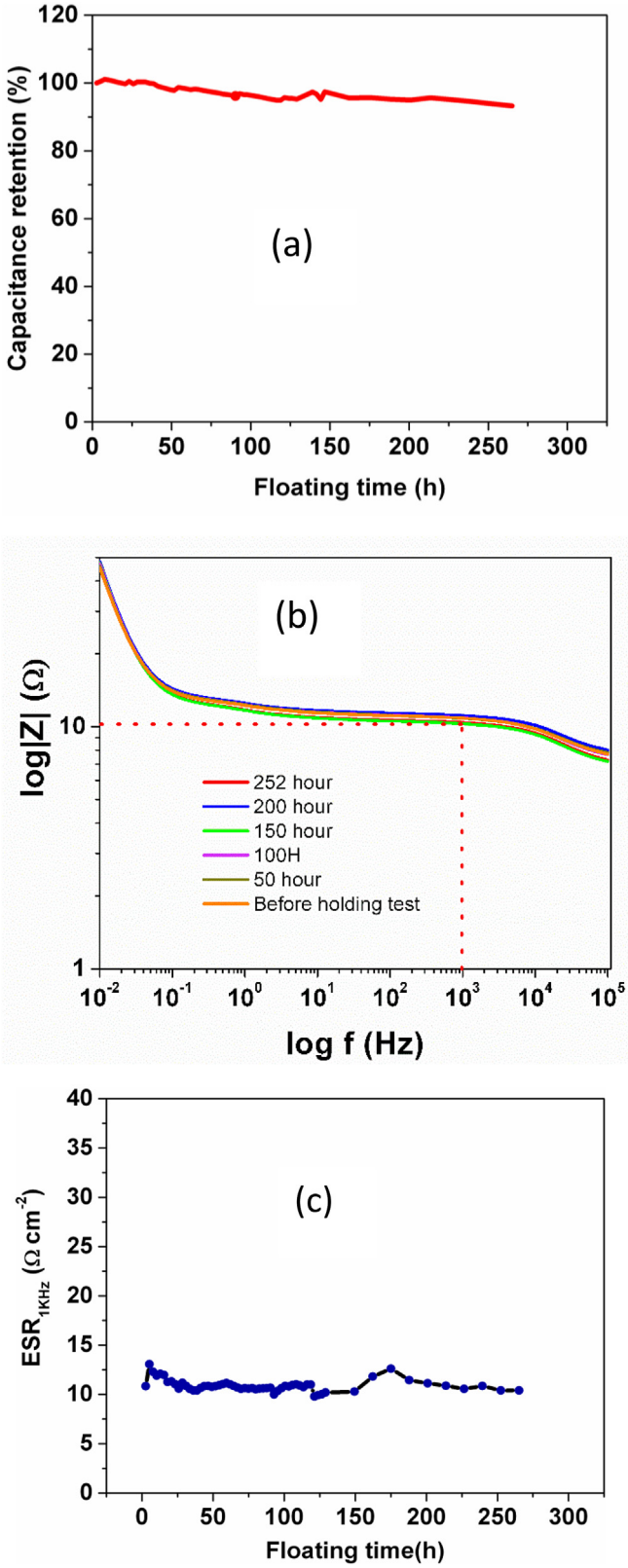

Fig. 5. Floating voltage hold test done at 4.2 V for 250 h showing, (a) Capacitance retention measured intermittently as a function of holding time, (b) Change in Bode plot during the holding test, (c) Change in ESR as a function of holding time; ESR measured using impedance at 1 KHz.

evidence of coalescence behavior. Fig. 2d show Raman spectra with two distinct characteristic D-band and G-band (E_{2g} graphite mode) at 1360 and 1600 cm^{-1} respectively. The intensity ratio, I_D/I_G was ~0.9 and the L_a (longitudinal crystallite size parallel to the a-axis) based on Raman was 4.9 nm. It is to be noted that functionalization can further affect the intensity of D-band. However, the significant curvature of the graphene domains in the onions as seen in TEM shows that the crystallite growth in the longitudinal direction was significantly less than the c-axis direction.

Fig. 3a shows de-lithiation profile of a prelithiated anode at different current densities ranging from 0.01V to 3V vs Li^+/Li. Carbon onion exhibits two distinct regions that include a flat plateau below ~0.2 V vs Li^+/Li and a slopy region from 0.2V vs Li^+/Li to 3V vs Li^+/Li. These regions correspond to lithium intercalation/deintercalation and electrochemical adsorption/desorption phenomena, respectively. The total delithiation capacity was 592 mAh/g at 100 mA/g and with 100x increase in current density to 10 A/g, the capacity reduced to 194 mAh/g which is still sufficiently high for design of ultra-high rate lithium ion capacitors. In addition, as the current density increased from 100 mA/g to 10 A/g, we saw slight voltage shift in the flat region due to increase in mass transfer resistance at high current density. The superior rate performance of the anode can also be seen when compared with various

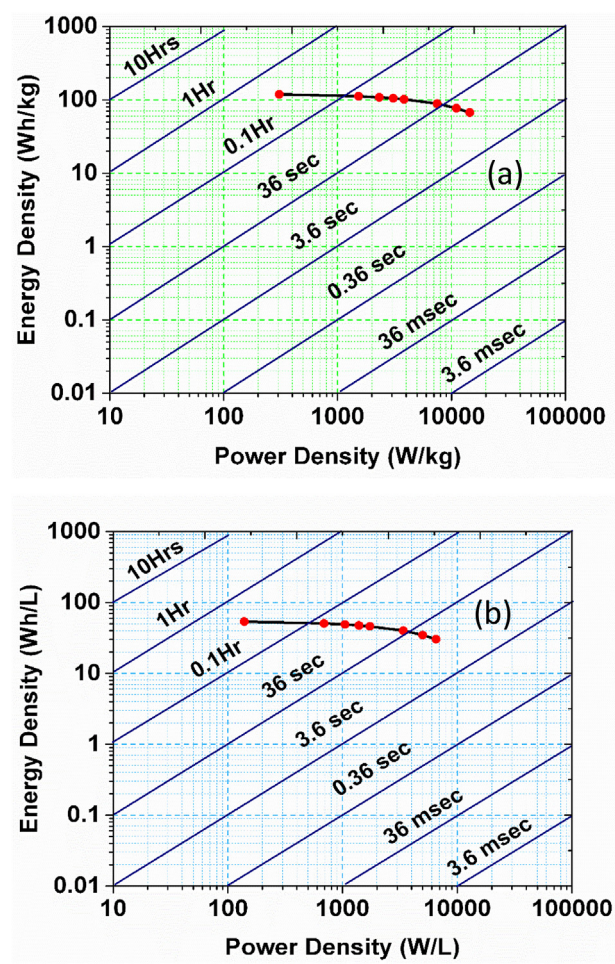

Fig. 6. (a) Gravimetric and (b) Volumetric Ragone plot of the PFA_Ph//CCO (based on active mass and volume of two electrodes).

nanostructured carbon anodes reported in the literature as shown in Fig. 3b.

Fig. 4a shows constant current charge/discharge profile when the cell was cycled between 2.2 V and 4 V at 2 A/g. At this current density, discharge time of the capacitor was 25s which corresponds to 144 C-rate. Fig. 4b shows the cycling performance of LIC device made using carbon onion anode and PFA_Ph carbon cathode. Device also showed excellent cyclability with 80% capacitance retention of 80% over 21000 cycles. Moreover, an energy efficiency of 91% was observed during this cycling test We believe that high cyclability and rate performance of the device was facilitated by the formation of thin and stable solid electrolyte interface (SEI) on carbon onion anode during pre-lithiation step (short circuiting approach). Fig. 4c shows Nyquist plot for LIC device before and after charge-discharge test. The presence of a small semicircle at intermediate frequency is due to the contribution from interfacial resistance and thin SEI layer formation on the anode. The total resistance from these phenomena which also include the electrolyte resistance was ~7.9 Ω cm^2. The small overall resistance of the device can be primarily attributed to coalescence and interparticle connectivity of the graphitic carbon onions. Also, pre-lithiation of carbon onion anode by short circuiting approach allowed us to form stable SEI which does not considerably change or grow during long term cycling test. The bimodal porosity of PFA_Ph cathode also has a positive effect on achieving high device cyclability and rate performance. The time constant of the fabricated capacitor was ~1.45s as shown in Fig. 4d.

We also performed the accelerated floating voltage test to confirm the high voltage stability of the device. Fig. 5a shows that capacitor had 93% capacitance retention when held at 4.2V for over 250 h. Fig. 5b shows the bode plot during floating voltage test and we saw very little change in the impedance over the entire frequency range measured intermittently during the floating test. We also saw minimal change in ESR (magnitude of impedance at 1 KHz) as shown in Fig. 5c.

Fig. 6 (a) shows gravimetric Ragone plot of the capacitor cycled between 2.2 V and 4.2V. A maximum energy density of 120 Wh/Kg was achieved based on active mass of both electrodes at 308 W/kg. The capacitor was able to deliver 77 Wh/kg when the power density was increased to 11 kW/kg. At a very high power density of 14.5 kW/kg, the capacitor was still able to deliver an energy density of 67 Wh/kg which corresponded to a charge/discharge time of ~17 s. This is among the highest rate performance reported for all carbon based lithium ion capacitors as summarized in Table 2. Based on the bulk density of PFA_Ph (0.48 g/cc) and carbon onion anode (0.65 g/cc) and considering mass ratio of 2:1 (cathode/anode), the capacitor showed maximum volumetric energy density of 53.47 Wh/L at power density of 139.28 W/L and at a higher power density of 6.6 kW/L, the cell showed volumetric energy density of 30.6 Wh/L as shown in Fig. 6b. Table 3 shows a comparison of the volumetric and gravimetric of the PFA_Ph/CCO cell with those of the recently reported symmetric and asymmetric supercapacitors. The volumetric energy densities are normalized by the volume of the two electrodes.

In order to evaluate the performance of the device at the elevated temperature, we performed temperature study ranging from 25 to 60 °C. Fig. 7a shows the specific capacitance vs cycle number when the device cycled between 2.2 V and 4 V at 2 A/g at 3 different temperatures: 40 °C, 50 °C and 60 °C, respectively. We see slight increase in capacitance values with increasing temperature. This phenomenon can be explained by increased motion of cation (Li^+) and anion (PF_6^-) motion at high temperature leading to ease of ion diffusion in the pore structure as well as intercalation/de-intercalation. To further evaluate the performance of device at 60 °C, we did additional 1000 cycles demonstrating good capacitance retention and an energy efficiency >90%. as shown in Fig. 7b.

Table 2
Literature comparison showing maximum energy, power densities, and cycling stability of various Lithium ion hybrid capacitors.

Supercapacitor system	Voltage Window (V)	Cathode to Anode mass ratio (total mass)	Energy density (Wh kg^{-1})	Power density (W kg^{-1})	Cycling number	Capacitance retention ratio (%)	Ref.
PFA_Ph//CCO	2.2–4.2	2:1 (7 mg)	129 60	377 10000	21000 (2 Ag^{-1})	80	This work
APDC//VN/RGO	0–4	4:1 (5 mg)	162 64	200 10000	1000 (2 A g^{-1})	83	Ref [30]
URGO//Graphite	2–4	1:1 (4 mg)	106 85	84 4200	1000 (0.14 Ag^{-1})	99	Ref [9]
PdCs//AMC	0.5–4	~2:1 (1.9 mg)	133 42	210 11200	5000 (5 A g^{-1})	81.8	Ref [31]
Carbon sphere//B–Si/C	2–4.5	2:1 (6 mg)	128 89	1229 9704	6000 (1.6 A g^{-1})	70	Ref [32]
N-doped AC//Si/C	2–4.5	2:1	230 141	1747 30127	8000 (1.6 A g^{-1})	76.3	Ref [8]
URGO//modified graphite	2–4	2:1 (3 mg)	135 105	50 1500	3500 (0.138A g^{-1})	97	Ref [33]
SFAC//MCMB	2–4	1:1	83 41	128 5718	1000 (0.5A g^{-1})	92	Ref [34]
AC//MWCNTs	2–4	1:1 (3.64 mg)	96 36	150 4035	1000 (0.4A g^{-1})	89	Ref [35]
AC//N-doped hard carbon	2–4	2.5:1 (2.8 mg)	28.5 13.1	348 6940	5000 (0.5 A g^{-1})	97	Ref [36]
AC//hard carbon	1.5–3.9	1.6–1 (3.9)	80 60	150 ~2200	10000	83	Ref [37]
PF16//FRGO (both graphene based electrodes)	0–4.2	3.5:1	148 71.5	141 7800	3000 (~1.86 A g^{-1})	~80	Ref [38]
AC//Graphdiyne	2–4	2:1	112.2 95.1	400.1 1000.4	1000	94.7	Ref [39]
AC//HC	1.5–4.2		100 22	150 8000	1000	94	Ref [40]
carbon fibers//TiNb2O7@carbon	0.8–3.2	2.3:1	110.4 20	99.58 5464	1500 (0.2 A g^{-1})	77	Ref [41]

Table 3
Volumetric and gravimetric energy density comparison of both symmetric and asymmetric supercapacitors reported in the literature.

Materials	Density (g cm^{-3})	Electrolyte	Current Density (A g^{-1})	Eg (W h kg^{-1})	Ev (W h L^{-1})	Ref.
PFA_Ph/CCO (This work)	0.5	LiPF6(EC/DMC)	1	102	46	This work
AC	0.5	EMIMBF4	1	88	44	[42]
Cu modified AC	0.8	TEATFB	0.2	43.9	34.7	[43]
PF15G-HA	0.4	TEABF4/AN	1	51	20.2	[44]
PF15G-HA	0.4	EMIMBF4	1	98	38.8	[44]
MHCN	0.8	TEABF4/AN	0.5	22.4	17.3	[45]
EM-CCG	1.3	EMIMBF4/AN	0.1	47.9	59.9	[46]
aMEGO	0.4	BMIM BF4/AN	2.8	70	26.5	[47]
PFA_Ph	0.5	BMIM BF4	1	55.4	26.6	[23]
aMEGO	0.6	EMIM TFSI/AN	2.1	74	44	[48]
HPGM	1.6	6 M KOH	0.1	8.3	13.1	[49]
HPGM	1.6	TEABF4/AN	0.1	23.5	37.1	[49]
3D HPG	0.6	TEABF4/PC	1	38	22	[50]
Holey graphene	0.7	EMIMBF4/AN	1	127	90	[51]
Graphene/CNT film	1.1	EMIMBF4	0.5	110.6	117.2	[52]
Single-walled CNTs arrays	0.5	Et4NBF4/PC	1	94	47	[53]
Carbide derived carbon	0.5	EMIMTFSI	0.3	50	26.5	[29]
Chemically reduced graphene	0.5	Et4NBF4/AN	1.33	21.5	10.7	[54]
Curved graphene	0.3	EMIMBF4	1	85.6	25.7	[55]
Compressed a-MEGO	0.8	BMIMBF4/AN	1.2	63	48	[56]
asMEGO	0.5	EMIM TFSI/AN	1.1	55	25	[48]

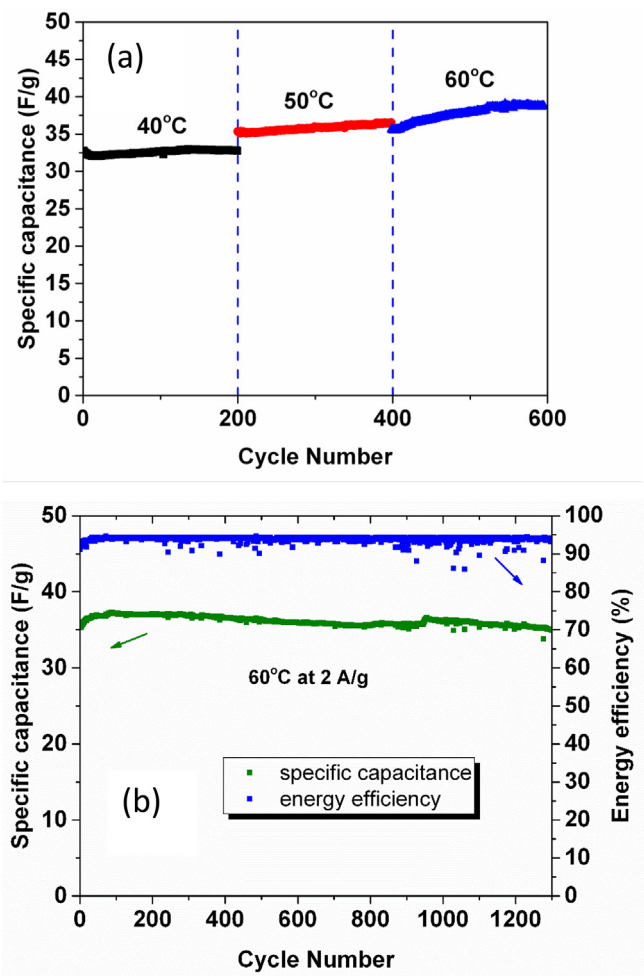

Fig. 7. (a) Specific capacitance as a function of cycle number at 2 A/g at different temprature when cycled between 2.2V and 4 V, and (b) additional 1000 cycles at 60°C.

4. Conclusions

Coalesced carbon onion based anode exhibited excellent electron and ion transport to facilitate fast electrochemical interactions with lithium ions and significantly improve the rate performance of LIC. The capacitors fabricated using the carbon onion anode and polymer derived carbon cathode with hierarchical pore structure demonstrated energy efficiencies >90% with 80% capacitance retention over 21000 cycles at room temperature and good cyclability at 60 °C at a current density of 2A/g. This corresponded to a discharge time of 17s with deliverable energy and power densities of 67 Wh/kg and 14.5 kW/kg, respectively.

Acknowledgments

This work was supported by the National Science Foundation ASSIST Nanosystems ERC under Award Number EEC-1160483. The authors would also like to acknowledge the financial support from NSF I/UCRC Center for Dielectrics and Piezoelectrics and ETCE Research Development Grant from The Pennsylvania State University. The authors would like to thank Materials Characterization Laboratory at University Park for providing access to various characterization facilities.

References

[1] J. Ding, W. Hu, E. Paek, D. Mitlin, Review of hybrid ion capacitors: from aqueous to lithium to sodium, Chem. Rev. 118 (14) (2018) 6457–6498.
[2] V. Khomenko, E. Raymundo-Piñero, F. Béguin, High-energy density graphite/AC capacitor in organic electrolyte, J. Power Sources 177 (2) (2008) 643–651.
[3] K. Naoi, S. Ishimoto, J.-i. Miyamoto, W. Naoi, Second generation 'nanohybrid supercapacitor': evolution of capacitive energy storage devices, Energy Environ. Sci. 5 (11) (2012) 9363–9373.
[4] Z. Yang, J. Ren, Z. Zhang, X. Chen, G. Guan, L. Qiu, Y. Zhang, H. Peng, Recent advancement of nanostructured carbon for energy applications, Chem. Rev. 115 (11) (2015) 5159–5223.
[5] I. Lahiri, W. Choi, Carbon nanostructures in lithium ion batteries: past, present, and future, Crit. Rev. Solid State Mater. Sci. 38 (2) (2013) 128–166.
[6] B. Li, J. Zheng, H. Zhang, L. Jin, D. Yang, H. Lv, C. Shen, A. Shellikeri, Y. Zheng, R. Gong, Electrode materials, electrolytes, and challenges in nonaqueous lithium-ion capacitors, Adv. Mater. (2018) 1705670.
[7] P. Simon, Y. Gogotsi, Materials for electrochemical capacitors, Nat. Mater. 7 (11) (2008) 845–854.
[8] B. Li, F. Dai, Q. Xiao, L. Yang, J. Shen, C. Zhang, M. Cai, Nitrogen-doped activated carbon for a high energy hybrid supercapacitor, Energy Environ. Sci. 9 (1) (2016) 102–106.

[9] J.H. Lee, W.H. Shin, M.-H. Ryou, J.K. Jin, J. Kim, J.W. Choi, Functionalized graphene for high performance lithium ion capacitors, ChemSusChem 5 (12) (2012) 2328–2333.
[10] H. Buqa, D. Goers, M. Holzapfel, M.E. Spahr, P. Novák, High rate capability of graphite negative electrodes for lithium-ion batteries, J. Electrochem. Soc. 152 (2) (2005) A474–A481.
[11] J.B. Habedank, L. Kraft, A. Rheinfeld, C. Krezdorn, A. Jossen, M.F. Zaeh, Increasing the discharge rate capability of lithium-ion cells with laser-structured graphite anodes: modeling and simulation, J. Electrochem. Soc. 165 (7) (2018) A1563–A1573.
[12] S.-S. Hou, D.-H. Chung, T.-H. Lin, High-yield synthesis of carbon nano-onions in counterflow diffusion flames, Carbon 47 (4) (2009) 938–947.
[13] D.-H. Chung, T.-H. Lin, S.-S. Hou, Flame synthesis of carbon nano-onions enhanced by acoustic modulation, Nanotechnology 21 (43) (2010) 435604.
[14] X.H. Chen, F.M. Deng, J.X. Wang, H.S. Yang, G.T. Wu, X.B. Zhang, J.C. Peng, W.Z. Li, New method of carbon onion growth by radio-frequency plasma-enhanced chemical vapor deposition, Chem. Phys. Lett. 336 (3) (2001) 201–204.
[15] A.G. Nasibulin, A. Moisala, D.P. Brown, E.I. Kauppinen, Carbon nanotubes and onions from carbon monoxide using Ni (acac) 2 and Cu (acac) 2 as catalyst precursors, Carbon 41 (14) (2003) 2711–2724.
[16] Y. Yang, X. Liu, B. Xu, Fe-encapsulating carbon nano onionlike fullerenes from heavy oil residue, J. Mater. Res. 23 (5) (2008) 1393–1397.
[17] C. Zhang, J. Li, C. Shi, E. Liu, X. Du, W. Feng, N. Zhao, The efficient synthesis of carbon nano-onions using chemical vapor deposition on an unsupported Ni–Fe alloy catalyst, Carbon 49 (4) (2011) 1151–1158.
[18] T. Gorelik, S. Urban, F. Falk, U. Kaiser, U. Glatzel, Carbon onions produced by laser irradiation of amorphous silicon carbide, Chem. Phys. Lett. 373 (5–6) (2003) 642–645.
[19] T. Kobayashi, T. Sekine, H. He, Formation of carbon onion from heavily shocked SiC, Chem. Mater. 15 (14) (2003) 2681–2683.
[20] J.Y. Huang, H. Yasuda, H. Mori, Highly curved carbon nanostructures produced by ball-milling, Chem. Phys. Lett. 303 (1) (1999) 130–134.
[21] F.-D. Han, B. Yao, Y.-J. Bai, Preparation of carbon nano-onions and their application as anode materials for rechargeable lithium-ion batteries, J. Phys. Chem. C 115 (18) (2011) 8923–8927.
[22] M.E. Plonska-Brzezinska, L. Echegoyen, Carbon nano-onions for supercapacitor electrodes: recent developments and applications, J. Mater. Chem. 1 (44) (2013) 13703–13714.
[23] A.R. Aref, C.-C. Chou, R. Rajagopalan, C. Randall, Bimodal porous carbon electrodes derived from polyfurfuryl alcohol/phloroglucinol for ionic liquid based electrical double layer capacitors, J. Mater. Res. 33 (9) (2017) 1189–1198.
[24] A.R. Aref, R. Rajagopalan, C.A. Randall, High-voltage stability of ionic-liquid-based electrochemical double layer capacitors with a bimodal porous carbon electrode, ChemElectroChem 5 (22) (2018) 3460–3467.
[25] C.L. Burket, R. Rajagopalan, A.P. Marencic, K. Dronvajjala, H.C. Foley, Genesis of porosity in polyfurfuryl alcohol derived nanoporous carbon, Carbon 44 (14) (2006) 2957–2963.
[26] M. Peer, A. Qajar, R. Rajagopalan, H.C. Foley, Synthesis of carbon with bimodal porosity by simultaneous polymerization of furfuryl alcohol and phloroglucinol, Microporous Mesoporous Mater. 196 (2014) 235–242.
[27] P. Llewellyn, F. Rodriquez-Reinoso, J. Rouqerol, N. Seaton, Is the BET equation applicable to microporous adsorbents? Stud. Surf. Sci. Catal. 160 (2007) 49–56.
[28] C.L. Berhaut, D. Lemordant, P. Porion, L. Timperman, G. Schmidt, M. Anouti, Ionic association analysis of LiTDI, LiFSI and LiPF 6 in EC/DMC for better Li-ion battery performances, RSC Adv. 9 (8) (2019) 4599–4608.
[29] C. Largeot, C. Portet, J. Chmiola, P.-L. Taberna, Y. Gogotsi, P. Simon, Relation between the ion size and pore size for an electric double-layer capacitor, J. Am. Chem. Soc. 130 (9) (2008) 2730–2731.
[30] R. Wang, J. Lang, P. Zhang, Z. Lin, X. Yan, Fast and large lithium storage in 3D porous VN nanowires–graphene composite as a superior anode toward high-performance hybrid supercapacitors, Adv. Funct. Mater. 25 (15) (2015) 2270–2278.
[31] W.S.V. Lee, X. Huang, T.L. Tan, J.M. Xue, Low Li+ insertion barrier carbon for high energy efficient lithium-ion capacitor, ACS Appl. Mater. Interfaces 10 (2) (2018) 1690–1700.
[32] R. Yi, S. Chen, J. Song, M.L. Gordin, A. Manivannan, D. Wang, High-performance hybrid supercapacitor enabled by a high-rate Si-based anode, Adv. Funct. Mater. 24 (47) (2014) 7433–7439.
[33] J.H. Lee, W.H. Shin, S.Y. Lim, B.G. Kim, J.W. Choi, Modified graphite and graphene electrodes for high-performance lithium ion hybrid capacitors, Materials for Renewable and Sustainable Energy 3 (1) (2014) 22.
[34] Z. Yang, H. Guo, X. Li, Z. Wang, Z. Yan, Y. Wang, Natural sisal fibers derived hierarchical porous activated carbon as capacitive material in lithium ion capacitor, J. Power Sources 329 (2016) 339–346.
[35] M. Cai, X. Sun, Y. Nie, W. Chen, Z. Qiu, L. Chen, Z. Liu, H. Tang, Electrochemical performance of lithium-ion capacitors using pre-lithiated multiwalled carbon nanotubes as anode, Nano 12 (04) (2017) 1750051.
[36] X. Han, P. Han, J. Yao, S. Zhang, X. Cao, J. Xiong, J. Zhang, G. Cui, Nitrogen-doped carbonized polyimide microsphere as a novel anode material for high performance lithium ion capacitors, Electrochim. Acta 196 (2016) 603–610.
[37] J.-H. Kim, J.-S. Kim, Y.-G. Lim, J.-G. Lee, Y.-J. Kim, Effect of carbon types on the electrochemical properties of negative electrodes for Li-ion capacitors, J. Power Sources 196 (23) (2011) 10490–10495.
[38] T. Zhang, F. Zhang, L. Zhang, Y. Lu, Y. Zhang, X. Yang, Y. Ma, Y. Huang, High energy density Li-ion capacitor assembled with all graphene-based electrodes, Carbon 92 (2015) 106–118.
[39] H. Du, H. Yang, C. Huang, J. He, H. Liu, Y. Li, Graphdiyne applied for lithium-ion capacitors displaying high power and energy densities, Nanomater. Energy 22 (2016) 615–622.
[40] J. Ajuria, E. Redondo, M. Arnaiz, R. Mysyk, T. Rojo, E. Goikolea, Lithium and sodium ion capacitors with high energy and power densities based on carbons from recycled olive pits, J. Power Sources 359 (2017) 17–26.
[41] X. Wang, G. Shen, Intercalation pseudo-capacitive TiNb2O7@carbon electrode for high-performance lithium ion hybrid electrochemical supercapacitors with ultrahigh energy density, Nanomater. Energy 15 (2015) 104–115.
[42] L. Zhang, F. Zhang, X. Yang, K. Leng, Y. Huang, Y. Chen, High-performance supercapacitor electrode materials prepared from various pollens, Small 9 (8) (2013) 1342–1347.
[43] L. Zhang, S.L. Candelaria, J. Tian, Y. Li, Y.-x. Huang, G. Cao, Copper nanocrystal modified activated carbon for supercapacitors with enhanced volumetric energy and power density, J. Power Sources 236 (2013) 215–223.
[44] L. Zhang, F. Zhang, X. Yang, G. Long, Y. Wu, T. Zhang, K. Leng, Y. Huang, Y. Ma, A. Yu, Porous 3D graphene-based bulk materials with exceptional high surface area and excellent conductivity for supercapacitors, Sci. Rep. 3 (2013) 1408.
[45] G.P. Hao, A.H. Lu, W. Dong, Z.Y. Jin, X.Q. Zhang, J.T. Zhang, W.C. Li, Sandwich-type microporous carbon nanosheets for enhanced supercapacitor performance, Advanced Energy Materials 3 (11) (2013) 1421–1427.
[46] X. Yang, C. Cheng, Y. Wang, L. Qiu, D. Li, Liquid-mediated dense integration of graphene materials for compact capacitive energy storage, Science 341 (6145) (2013) 534–537.
[47] Y. Zhu, S. Murali, M.D. Stoller, K. Ganesh, W. Cai, P.J. Ferreira, A. Pirkle, R.M. Wallace, K.A. Cychosz, M. Thommes, Carbon-based supercapacitors produced by activation of graphene, Science 332 (6037) (2011) 1537–1541.
[48] T. Kim, G. Jung, S. Yoo, K.S. Suh, R.S. Ruoff, Activated graphene-based carbons as supercapacitor electrodes with macro- and mesopores, ACS Nano 7 (8) (2013) 6899–6905.
[49] Y. Tao, X. Xie, W. Lv, D.-M. Tang, D. Kong, Z. Huang, H. Nishihara, T. Ishii, B. Li, D. Golberg, Towards ultrahigh volumetric capacitance: graphene derived highly dense but porous carbons for supercapacitors, Sci. Rep. 3 (2013) 2975.
[50] Y. Li, Z. Li, P.K. Shen, Simultaneous formation of ultrahigh surface area and three-dimensional hierarchical porous graphene-like networks for fast and highly stable supercapacitors, Adv. Mater. 25 (17) (2013) 2474–2480.
[51] Y. Xu, Z. Lin, X. Zhong, X. Huang, N.O. Weiss, Y. Huang, X. Duan, Holey graphene frameworks for highly efficient capacitive energy storage, Nat. Commun. 5 (2014) 4554.
[52] D.T. Pham, T.H. Lee, D.H. Luong, F. Yao, A. Ghosh, V.T. Le, T.H. Kim, B. Li, J. Chang, Y.H. Lee, Carbon nanotube-bridged graphene 3D building blocks for ultrafast compact supercapacitors, ACS Nano 9 (2) (2015) 2018–2027.
[53] A. Izadi-Najafabadi, S. Yasuda, K. Kobashi, T. Yamada, D.N. Futaba, H. Hatori, M. Yumura, S. Iijima, K. Hata, Extracting the full potential of single-walled carbon nanotubes as durable supercapacitor electrodes operable at 4 V with high power and energy density, Adv. Mater. 22 (35) (2010) E235–E241.
[54] M.D. Stoller, S. Park, Y. Zhu, J. An, R.S. Ruoff, Graphene-based ultracapacitors, Nano Lett. 8 (10) (2008) 3498–3502.
[55] C. Liu, Z. Yu, D. Neff, A. Zhamu, B.Z. Jang, Graphene-based supercapacitor with an ultrahigh energy density, Nano Lett. 10 (12) (2010) 4863–4868.
[56] S. Murali, N. Quarles, L.L. Zhang, J.R. Potts, Z. Tan, Y. Lu, Y. Zhu, R.S. Ruoff, Volumetric capacitance of compressed activated microwave-expanded graphite oxide (a-MEGO) electrodes, Nanomater. Energy 2 (5) (2013) 764–768.